

Article

Environmentally Friendly and Cost-Effective Synthesis of Carbonaceous Particles for Preparing Hollow SnO₂ Nanospheres and their Bifunctional Li-Storage and Gas-Sensing Properties

Yingyi Ding ¹, Ping Zhou ^{2,3}, Tianli Han ^{1,*} and Jinyun Liu ^{1,*} 

¹ Key Laboratory of Functional Molecular Solids, Ministry of Education, College of Chemistry and Materials Science, Anhui Normal University, Wuhu, Anhui 241000, China; yokiding1@ahnu.edu.cn

² Institute of Intelligent Machines, Chinese Academy of Sciences, Hefei 230031, China; lenazp@mail.ustc.edu.cn

³ Department of Chemistry, University of Science and Technology of China, Hefei 230026, China

* Correspondence: hantianli@ahnu.edu.cn (T.H.); jyliu@iim.ac.cn (J.L.)

Received: 9 March 2020; Accepted: 21 March 2020; Published: 23 March 2020



Abstract: The templated preparation of hollow nanomaterials has received broad attention. However, many templates are expensive, environmentally-harmful, along with involving a complicated preparation process. Herein, we present a cost-effective, environmentally friendly and simple approach for making carbonaceous particles which have been demonstrated as efficient templates for preparing hollow nanospheres. Natural biomass, such as wheat or corn, is used as the source only, and thus other chemicals are not needed. The carbonaceous particles possess abundant hydroxyl and carboxyl groups, enabling them to efficiently adsorb metal ions in solution. The prepared SnO₂ hollow spheres were used in a lithium-ion (Li-ion) battery anode, and as the sensing layer of a gas sensor, respectively. After charge–discharge for 200 times at a rate of 1 C, the anodes exhibit a stable capacity of 500 mAh g^{−1}, and a Coulombic efficiency as high as 99%. In addition, the gas sensor based on the SnO₂ hollow spheres shows a high sensing performance towards ethanol gas. It is expected that the presented natural biomass-derived particles and their green preparation method will find more applications for broad research fields, including energy-storage and sensors.

Keywords: nanostructure; metal oxide; templated preparation; Li-ion battery; capacity

1. Introduction

Since the discovery of fullerenes and carbon nanotubes, carbonaceous materials have attracted considerable attention, owing to their fascinating properties and applications [1–3]. Among them, particles as an important member of the carbonaceous family have received more and more interest because of their wide applications in many fields, such as lubricants and catalyst supports [4–6]. In addition, carbonaceous particles can be applied as templates for fabricating a large variety of hollow and porous spheres, including metal oxides (e.g., ZnO, TiO₂, SnO₂, CeO₂, etc.) which could greatly enhance their performance in electronic devices [7–12]. Recently, the preparation of carbonaceous particles, and further exploring their potential applications, have attracted extensive attention [13,14]. Several methods have been investigated, e.g., chemical vapor deposition, a hydrothermal approach, the carbonization of polymers and pyrolysis [15,16]. Regarding to the environment issues, “green” approaches have been of great interest. Several efforts focus on using environmentally friendly reagents and reducing the preparation steps. For instance, Zhang et al. reported a multiscale recombined

porous Si/C composites, prepared via a simple Ag-assisted chemical etching process [17]. In their study, chitosan was chosen as the carbon source, which was nontoxic and biodegradable.

Xiao and co-workers showed a convenient and green strategy for the synthesis of highly luminescent and water-soluble carbon dots, by carbonizing precursors, such as Bovine serum albumin nanoparticles, in water solution [18]. Interestingly, Hao et al. developed a one-pot green synthesis of luminescent carbon dots and carbon-coated metal (Au, Pt, Pd) particles by using the vitamin B2 salt as the carbon source and reducing agent [19]. In addition, Ren et al. in situ fabricated Ru, Fe-containing zinc–trimesic acid metal organic framework fibers, then they were able to get the RuFe@Fe₂O₃ particles confined into mesoporous carbon nanofibers by using one-step pyrolysis [20]. The thermal treatment and chemicals used for reactions were simplified significantly. Similar green approaches were also widely studied [21]. In spite of those achievements, high temperature, expensive instruments and chemicals, and/or toxic reagents are commonly required. Taking the commonly used polymethyl methacrylate (PMMA) particle template as an example, it is usually prepared through a polymerization route [22]. Usually, methyl methacrylate is used as the polymer monomer, while an initiator (such as potassium peroxydisulfate) and an emulgator (sodium dodecyl benzene sulfonate) are also added into an emulsion system. Under controlled polymerization temperature and stirring speed, PMMA particles are obtained. As seen, the procedure is high-cost, and multiple, complicated steps with poisonous chemicals are needed. Currently, it requires a preparation route of template particles, which is cost-effective, simple and environmentally friendly.

Herein, we present a natural biomass-derived approach that is cost-effective, environmentally friendly and simple for the preparation of carbonaceous particles. The particles were further used as templates to prepare hollow metal oxide spheres. In our investigation, natural wheat and corn were used as our carbon source, respectively, as shown in Figure 1. Compared to the conventional PMMA templates and their preparation approach indicated above, the presented route is completely “green”, in which other chemicals are unnecessary during the hydrothermal synthesis. The carbon sources are low-cost; and the route is simple without complicated procedures and instruments. The carbonaceous particles were used as sacrificing templates for the fabrication of porous and hollow SnO₂, which is a representative transition metal oxide. The SnO₂ spheres-based Li-ion battery anodes exhibit a stable capacity of 500 mAh g⁻¹ when cycling at a rate of 1 C for 200 times, along with a stable Coulombic efficiency of about 99%. In addition, the sensor based on the SnO₂ possesses a good gas-sensing performance towards ethanol gas.

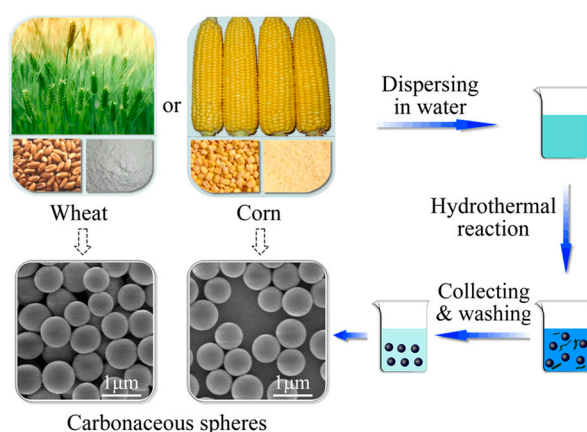


Figure 1. Illustration of the preparation of carbonaceous particles from natural biomass.

2. Experimental

2.1. Reagents and Solutions

All chemicals used in the study were of analytical grade, and were used without further purification. The wheat and corn were purchased from the China Oil and Foodstuffs Corporation (COFCO Corp.). Tin(IV) chloride ($\text{SnCl}_4 \cdot 5\text{H}_2\text{O}$) and chemicals used in sensors and batteries were bought from the Sinopharm Chemical Reagent Company.

2.2. Preparation of the Carbonaceous Particles

Firstly, wheat or corn was mechanically milled into powders (ca. 500 mesh). Then, 0.1 g of the wheat powders (or corn powders) were dispersed in 40 mL of distilled water by ultrasonication. The solution was transferred into a Teflon-sealed autoclave and maintained at 180 °C for 6 h. After the autoclave was cooled down naturally to room temperature, the products were collected by using centrifugation, and washed several times with distilled water. At last, the products were dried in an oven at 60 °C for further use.

2.3. Preparation of the Hollow SnO_2 Spheres

In order to prepare the porous hollow metal oxides by using the synthesized particles, 0.1 g of the carbonaceous particles were dispersed in 10 mL of ethanol by ultrasonication. Then, 1 mmol of $\text{SnCl}_4 \cdot 5\text{H}_2\text{O}$ was dissolved into the mixture obtained above. After being left statically at room temperature for 24 h, the precipitate was collected by centrifugation. The samples were put into an oven for drying at 50 °C. At last, the dried powders were annealed in a furnace at 500 °C for 1 h to remove the carbonaceous particles.

2.4. Characterizations

The samples were characterized on a Sirion-200 field emission scanning electron microscopy (FESEM, FEI, USA), a H-800 transmission electron microscopy (TEM, Hitachi, Japan) and an ESCALab MK II X-ray photoelectron spectrometer (XPS, Thermo Scientific, USA). The SEM was operated at an accelerating voltage of 5 kV. All of the samples were dispersed on Si substrates. For the TEM characterizations, the samples were dispersed in ethanol, then dropped onto Cu grids for further observation. The accelerating voltage of TEM was 200 kV. During XPS measurements, the binding energies in the XPS spectrum were calibrated by using that of C 1s (284.6 eV). The Fourier transform infrared (FTIR) spectrum was recorded on a IR-440 spectrometer (Shimadzu, Japan) from 4000 to 500 cm^{-1} . The samples (powders) were mixed with KBr, then ground and pressed into a small piece for measurement.

2.5. Energy-Storage Performance Study

The electrochemical properties of the prepared SnO_2 hollow spheres were measured by using a CR2032 coin-cell system. The electrode prepared by mixing SnO_2 (80 wt%), carbon black (10 wt%) and polyvinylidene fluoride binder (10 wt%) dissolved in N-methyl pyrrolidinone to form a slurry, which was then coated onto a Cu foil and dried in a vacuum at 110 °C. The substrates were tailored into circular pieces with a 14 mm-diameter. The SnO_2 anodes were set as working electrodes. A microporous polypropylene film was employed in the coin cell as the separator. Li foil was used as the counter electrode. Cells were assembled in a Super 1220/750 glovebox (Mikrouna, Germany) filled with Ar gas (O_2 and $\text{H}_2\text{O} < 0.01$ ppm). 1 M of LiPF_6 in a mixture of EC/DEC (1:1 by volume) was used as the electrolyte. The tests were conducted through the galvanostatic discharge-charge method on a CT-4008 battery tester (Shenzhen Neware Technology Co., Ltd, China).

2.6. Gas Sensor Fabrication and Gas-Sensing Property Measurements

At first, the gas sensors using the obtained SnO₂ as the sensing layer were constructed. The SnO₂ spheres were dispersed in ethanol by using ultrasonication for 10 min. Then, the slurry was coated onto the surface of an Al₂O₃ tube in which there was a Ni–Cr wire used as a heater. The sensors were dried at 50 °C under vacuum. Before each gas-sensing measurement, the sensors were aged at working conditions for two days, so that a stable and reliable performance could be obtained. During the gas-sensing tests, ethanol gas at concentrations of 10 ppm, 20 ppm, 30 ppm, 40 ppm, 150 ppm, 200 ppm and 250 ppm were employed as targets, respectively. All gas-sensing measurements were conducted at the same working temperature of gas sensors (~200 °C) and humidity of 60% RH. The tests were conducted by using a computer-controlled gas detecting system in which a Keithley 6487 picoamper/voltage sourcemeter was used as both the current recorder and power source.

3. Results and Discussion

The FESEM images of the samples prepared by using wheat and corn are presented in Figure 2a,c, respectively. The wheat- and corn-derived samples are similar in morphology, which is spherical with a narrow size distribution from 650 to 800 nm. This is confirmed by the TEM photographs, as shown in Figure 2b,d. The surface state and functional groups of particles were investigated by using XPS and FTIR. Taking the wheat-derived carbonaceous particle as an example, in the XPS spectrum (Figure 3a), the peaks at 284.6 eV, 285.9 eV, 287.1 eV and 288.5 eV are assigned to the carbon atoms bonded to graphitized carbon, C–OH groups, C–O–C and C=O groups, and O=C–O groups, respectively [23–25]. The surface of the carbonaceous particles is hydrophilic, because of the existence of the C–OH and O=C–O groups, and thus the products are unnecessary to be further functionalized before their use as templates to adsorb metal ions. Moreover, aromatization under the hydrothermal condition is demonstrated. It is further supported by the FTIR spectrum (Figure 3b), in which the carbonyl and hydroxyl groups were detected. In Figure 3b, the peak at 3413 cm⁻¹ is assigned to the O–H; while the ones at 1308 cm⁻¹ and 1271 cm⁻¹ correspond to the C–H group. Moreover, the peaks at 1700 cm⁻¹ and 1608 cm⁻¹ are indexed to the C=O and C=C [26,27], respectively, which are in good agreement with the XPS results shown above.

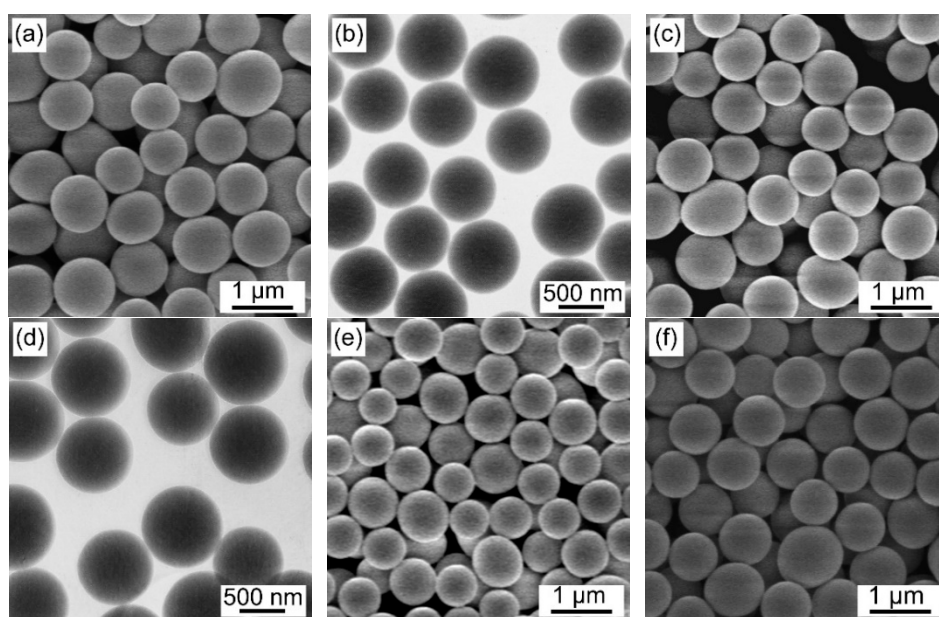


Figure 2. Field emission scanning electron microscopy (FESEM) images of the particles prepared using (a) wheat, (c) corn, (e) starch and (f) maltose. Transmission electron microscopy (TEM) photographs of the samples synthesized from (b) wheat and (d) corn.

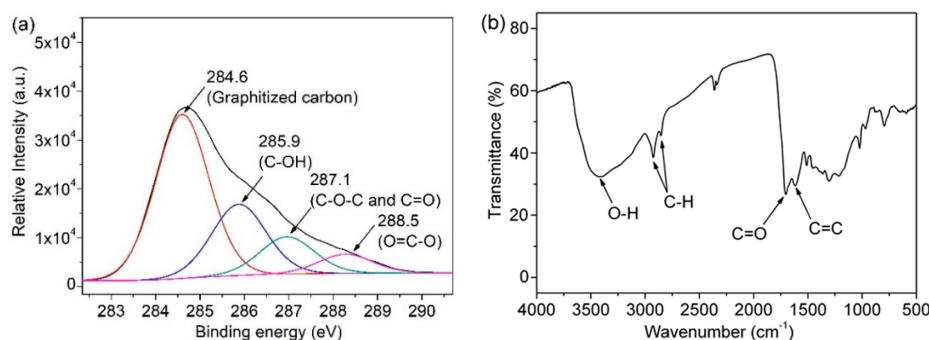


Figure 3. (a) X-ray photoelectron spectrometer (XPS) spectrum of the C1s region of wheat-derived carbonaceous particles. (b) Fourier transform infrared spectroscopy (FTIR) spectrum of the particles prepared from wheat.

On the basis of the study on XPS and FTIR spectra, the formation mechanism of carbonaceous particles derived from natural biomasses is explained as follows: Firstly, both wheat and corn are consisting of starch dominantly together, with a few saccharine components. Among various components in wheat, this starch and maltose are overwhelming, with percentages of ca. 75% and 8%, respectively. Under hydrothermal conditions, starch and saccharine are released into the solution. The dehydration and aromatization would occur, which are similar to the glucose [28,29], resulting in the formation of carbonaceous particles. In order to confirm this, pure starch and maltose were also employed as raw materials. The hydrothermal conditions are the same as those for wheat and corn. Figure 2e,f show the FESEM images of samples prepared from pure starch and maltose, respectively. They are close to the ones synthesized from wheat, supporting the suggested mechanism that starch and saccharine components would contribute to the formation of the carbonaceous particles.

Figure 4 shows the morphology and structure of the SnO₂ hollow spheres prepared by using the wheat-derived carbonaceous particle templates. It should be indicated that those SnO₂ spheres are presented as a demonstrating example. Under the same preparation procedures, similar SnO₂ spheres were also obtained by using the corn-derived carbonaceous particles. In Figure 4a, the samples exhibit a porous spherical morphology with a diameter of about 300 nm. Compared to the carbonaceous templates, the size of the hollow spheres is small. It is ascribed to the shrink of the carbonaceous particles during annealing, which is similar to some other reports [30,31]. The shell of the hollow spheres is assembled by nanoparticles, as seen from the high-magnification FESEM image (Figure 4b). The particles are about 20 nm-large without obvious morphology. In the TEM image (Figure 4c), the samples display a hollow structure with a shell thickness of ca. 20 nm, which is close to the size of the particles. It indicates that the shell of the spheres is assembled by monolayered nanoparticles. In order to confirm if there is some carbon residual within the SnO₂ spheres, we have used the pure carbonaceous particles (without adsorbing Sn(IV) ions) for calcination under the same annealing condition as the SnO₂ spheres. After the thermal treatment, no residual in the ceramic boat was observed. Therefore, it is considered that there is no residual carbon in the SnO₂ spheres after calcination.

Figure 5 shows the charge–discharge performance of the SnO₂ hollow spheres-based anodes. In Figure 5a, the plateaus at the discharge and charge curves are ascribed to the lithiation and delithiation. On the basis of the reaction mechanism of SnO₂, an alloying–dealloying mechanism would be dominated from the second cycle [32]. Cycling at a rate of 1 C (1 C equals to the complete charge or discharge of theoretical capacity of 782 mAh g^{−1} in 1 h), the SnO₂ anode exhibits a high first-cycle capacity of about 1200 mAh g^{−1}, which is ascribed to the formation of an unstable solid electrolyte interphase (SEI) [33,34]. In Figure 5b, during the subsequent cycles, the capacity decreases gradually. However, from the 30th cycle, the capacity becomes stable, indicating the formation of a stable SEI. After cycling for 200 times, the capacity remains exceeding 500 mAh g^{−1}, along with a high Coulombic efficiency of about 99%, indicating a good reversibility. This is ascribed to the hollow structure which enables the volume-change to be accommodated [35,36].

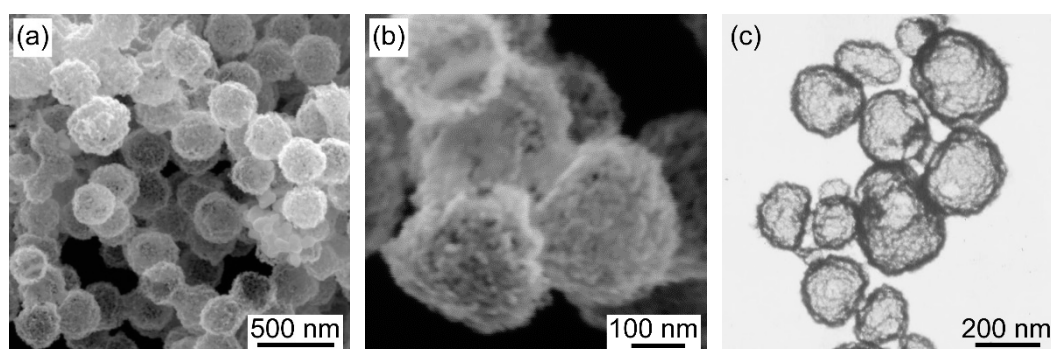


Figure 4. (a) Low- and (b) high-magnification FESEM and (c) TEM images of the SnO₂ spheres prepared by using the wheat-derived carbonaceous particles as template.

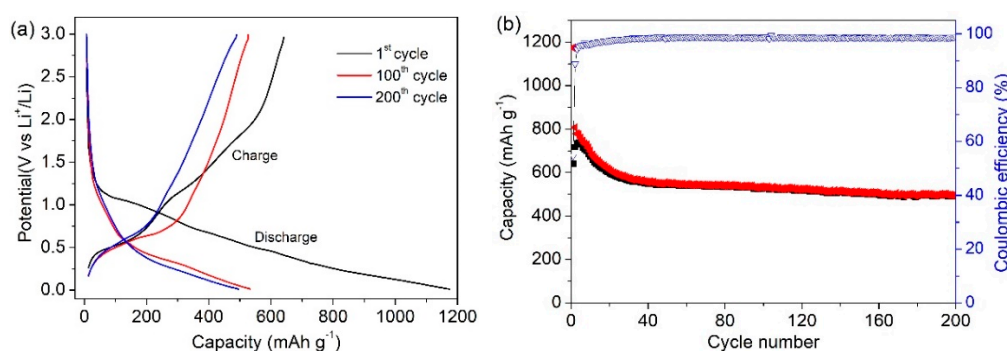


Figure 5. (a) Galvanostatic charge-discharge curves of the SnO₂ anode cycling at 1C. (b) Capacity and Coulombic efficiency versus cycle number.

Figure 6 displays the gas-sensing responses of the sensor towards ethanol gases. In Figure 6a, once the ethanol gas was injected into the detecting chamber, the current increased rapidly, indicating a short response time, which was commonly defined as the time for the sensor to achieve 90% of the total resistance-change. As seen from the real-time sensing curves, the response times of the sensor are about 8.5 s, 6.5 s, 4.5 s and 5 s for 10 ppm, 20 ppm, 30 ppm and 40 ppm ethanol gases, respectively. The fast response is attributed to the porous and hollow morphology and the nanospheres assembled by small nanoparticles. As for the sensing mechanism, this is explained as follows: In air ambient conditions, the oxygen is adsorbed on SnO₂, forming some negative ionic species, like O⁻ and O²⁻. Because of that, the electrons in SnO₂ would be captured, resulting in a high resistance. When ethanol gas is injected into the chamber, it will be oxidized by those ionic species on SnO₂, releasing the electrons and exhibiting a low resistance. In contrast, when the fresh gas was introduced to replace the target ethanol gas, the reversible reactions happened, resulting in the recovery of the current. For instance, for detecting 20 ppm ethanol, the resistance of the fresh gas sensor was $2.73 \times 10^6 \Omega$. While the target gas was injected into the chamber, the resistance decreased, and reached to about $0.21 \times 10^6 \Omega$ at the equilibrium stage.

In Figure 6b, the gas response is defined as the ratio of the current in pure air (I_{air}) and in the gas mixture (I_{gas}) at a constant voltage, which also reflects the change of resistances. In our investigation, the gas responses are about 7, 13, 22 and 39, when the concentrations of ethanol gases are 10 ppm, 20 ppm, 30 ppm and 40 ppm, respectively. The sensing response is competitive with some other materials, such as the TiO₂/SnO₂ nanofibers [37] and micro-/mesoporous SnO₂ spheres prepared by a solvothermal method [38]. It is ascribed to the nanosphere with a hollow and porous structure which provides a good contact and numerous sensing sites for gas molecules. In addition, during target gas injecting and releasing, the diffusion kinetics of the hollow spheres is fast, enabling short response and recovery times. Moreover, it is noted that the response curve is not in a linear profile. It is ascribed to this that the gas concentrations in the measurements would be not in the linear region

of the sensing performance. Since that, some relatively higher concentration gases were detected, as shown in Figure 6c,d. The responses of the sensor towards 200 ppm and 250 ppm gases become similar, indicating a saturation trend. Furthermore, compared to the sensing responses towards lower concentrations (10–40 ppm), it indicates that the sensor has a linear sensing range towards ethanol from about 30 to 150 ppm. It is expected that further investigations on humidity and stability would also be a benefit for the practical applications of the presented gas sensor.

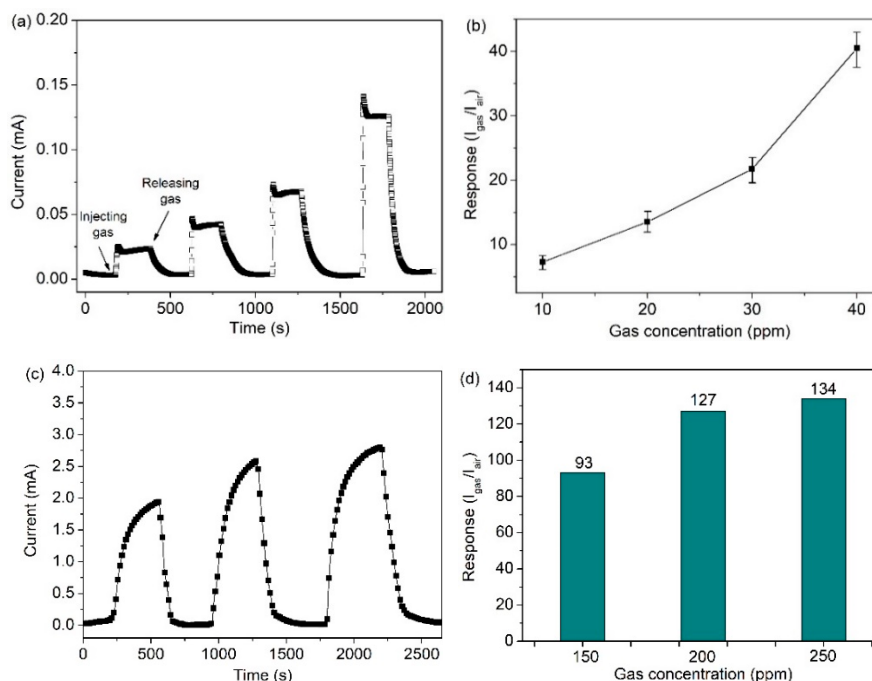


Figure 6. (a) Real-time gas-sensing curve and (b) the response performance of the sensor towards ethanol at concentrations of 10 ppm, 20 ppm, 30 ppm and 40 ppm. (c) Gas-sensing curves and (d) responses towards 150 ppm, 200 ppm and 250 ppm ethanol gas.

4. Conclusions

In summary, we present a cost-effective, environmentally friendly, and simple approach for preparing carbonaceous particles by using natural biomasses including wheat and corn. The particles can be easily used as templates for constructing hollow nanomaterials for energy-storage and gas-sensing applications. The abundant hydroxyl and carboxyl groups on the carbonaceous particles enable them to be suitable templates for the preparation of hollow nanostructures. The SnO₂ hollow spheres were prepared by using the carbonaceous particles as a demonstrating example. The SnO₂ anode-based Li-ion batteries exhibit a stable capacity of 500 mAh g⁻¹, and a Coulombic efficiency as high as 99% after charge–discharge 200 times at a rate of 1 C. In addition, the SnO₂-based gas sensor shows high response and short responding time towards ethanol. We believe that the presented wheat or corn-derived method for preparing carbonaceous particles could be potentially extended to many other natural biomasses. In addition, it is expected that the prepared carbonaceous particles are able to find more applications for a broad set of research fields.

Author Contributions: Investigation, Y.D., and J.L.; resources, T.H., and J.L.; writing—original draft preparation, Y.D., P.Z., T.H., and J.L.; supervision, J.L.; project administration, T.H., and J.L.; funding acquisition, J.L. All authors have read and agreed to the published version of the manuscript.

Funding: This research was funded by National Natural Science Foundation of China (grant number: 51672176), Science and Technology Major Project of Anhui Province (grant number: 18030901093), Key Research and Development Program of Wuhu (grant number: 2019YF07), Natural Science Research Project for Universities in Anhui Province (grant numbers: KJ2018ZD034 and KJ2019A0502), and Anhui Provincial Program for Innovation and Entrepreneurship of Returnees from Overseas (grant number: 2019LCX005). The APC was funded by Science and Technology Major Project of Anhui Province (grant number: 18030901093).

Conflicts of Interest: The authors declare no conflict of interest.

References

1. Yang, Z.F.; Tian, J.R.; Yin, Z.F.; Cui, C.J.; Qian, W. Carbon nanotube- and graphene-based nanomaterials and applications in high-voltage supercapacitor: A review. *Carbon* **2019**, *141*, 467–480. [[CrossRef](#)]
2. He, Y.; Zhao, L.D.; Wang, X.J.; Liu, L.Y.; Liu, H. Microstructured hybrid nanocomposite flexible piezoresistive sensor and its sensitivity analysis by mechanical finite-element simulation. *Nanotechnology* **2020**, *31*, 185502. [[CrossRef](#)] [[PubMed](#)]
3. Kim, T.; Cho, M.; Yu, K.J. Flexible and stretchable bio-integrated electronics based on carbon nanotube and graphene. *Materials* **2018**, *11*, 1163. [[CrossRef](#)]
4. He, X.Z. Techno-economic feasibility analysis on carbon membranes for hydrogen purification. *Sep. Purif. Technol.* **2017**, *186*, 117–124. [[CrossRef](#)]
5. Yan, D.Y.; Hu, H.; Gao, N.Y.; Ye, J.S.; Ou, H.S. Fabrication of carbon nanotube functionalized MIL-101(Fe) for enhanced visible-light photocatalysis of ciprofloxacin in aqueous solution. *Appl. Surf. Sci.* **2019**, *498*, 143836. [[CrossRef](#)]
6. Zhang, Y.X.; Cai, T.; Shang, W.J.; Liu, D.; Guo, Q.; Liu, S.G. Facile synthesis of photoluminescent inorganic-organic hybrid carbon dots codoped with B and N: Towards an efficient lubrication additive. *Dalton Trans.* **2017**, *46*, 12306–12312. [[CrossRef](#)]
7. Nowak, A.P. Composites of tin oxide and different carbonaceous materials as negative electrodes in lithium-ion batteries. *J. Solid State Electrochem.* **2018**, *22*, 2297–2304. [[CrossRef](#)]
8. Xiao, Q.; Wang, K.; Wang, X.X.; Huang, S.P.; Cai, N.N.; Li, N. Solvent-free template synthesis of SnO₂/C hybrid hollow spheres for superior lithium-sulfur batteries. *Mater. Chem. Phys.* **2020**, *239*, 122070. [[CrossRef](#)]
9. Kang, Y.R.; Li, Z.; Xu, K.; He, X.J.; Wei, S.X.; Cao, Y.M. Hollow SnO₂ nanospheres with single-shelled structure and the application for supercapacitors. *J. Alloy. Compd.* **2019**, *779*, 728–734. [[CrossRef](#)]
10. Hu, Q.; Huang, B.Y.; Li, Y.; Zhang, S.M.; Zhang, Y.X.; Hua, X.H.; Liu, G.; Li, B.S.; Zhou, J.Y.; Xie, E.Q.; et al. Methanol gas detection of electrospun CeO₂ nanofibers by regulating Ce³⁺/Ce⁴⁺ mole ratio via Pd doping. *Sens. Actuators B* **2020**, *307*, 127638. [[CrossRef](#)]
11. Liu, H.J.; Zhang, S.; Chen, Y.L.; Zhang, J.T.; Guo, P.; Liu, M.; Lu, X.Q.; Zhang, J.; Wang, Z.J. Rational design of TiO₂@nitrogen-doped carbon coaxial nanotubes as anode for advanced lithium ion batteries. *Appl. Surf. Sci.* **2018**, *458*, 1018–1025. [[CrossRef](#)]
12. Jin, L.F.; Chen, W.G.; Zhang, H.; Xiao, G.W.; Yu, C.T.; Zhou, Q. Characterization of reduced graphene oxide (rGO)-loaded SnO₂ nanocomposite and applications in C₂H₂ gas detection. *Appl. Sci.* **2017**, *7*, 19. [[CrossRef](#)]
13. Hu, L.J.; Qian, Z.X.; Gao, W.; Wang, X.F.; Tian, Y. Nanoengineering of uniform and monodisperse mesoporous carbon nanospheres mediated by long hydrophilic chains of triblock copolymers. *J. Mater. Sci.* **2020**, *55*, 2052–2067. [[CrossRef](#)]
14. Zhou, Q.Y.; Chen, W.H.; Jiang, X.; Liu, H.Y.; Ma, S.G.; Wang, B.D. Preparation of a novel nitrogen-containing graphitic mesoporous carbon for the removal of acid red 88. *Sci. Rep.* **2020**, *10*, 1353. [[CrossRef](#)] [[PubMed](#)]
15. Han, B.; Zhang, E.Y.; Cheng, G.; Zhang, L.J.; Wang, D.W.; Wang, X.K. Hydrothermal carbon superstructures enriched with carboxyl groups for highly efficient uranium removal. *Chem. Eng. J.* **2018**, *338*, 734–744. [[CrossRef](#)]
16. Huang, B.B.; Liu, Y.C.; Xie, Z.L. Biomass derived 2D carbons via a hydrothermal carbonization method as efficient bifunctional ORR/HER electrocatalysts. *J. Mater. Chem. A* **2017**, *5*, 23481–23488. [[CrossRef](#)]

17. Zhao, T.T.; Zhu, D.L.; Li, W.R.; Li, A.J.; Zhang, J.J. Novel design and synthesis of carbon-coated porous silicon particles as high-performance lithium-ion battery anodes. *J. Power Sources* **2019**, *439*, 227027. [[CrossRef](#)]
18. Yang, Q.X.; Wei, L.; Zheng, X.F.; Xiao, L.H. Single particle dynamic imaging and Fe³⁺ sensing with bright carbon dots derived from bovine serum albumin proteins. *Sci. Rep.* **2015**, *5*, 17727. [[CrossRef](#)]
19. Zhang, B.H.; Yang, Q.; Li, Z.H.; Hao, J.C. Green synthesis of luminescent carbon dots and carbon-coated metal particles: Two birds with one stone. *Colloid. Surface A* **2015**, *485*, 34–41. [[CrossRef](#)]
20. Yang, Y.; Yang, F.; Sun, C.J.; Zhao, H.R.; Hao, S.J.; Brown, D.E.; Zhang, J.; Ren, Y. Ru-Fe alloy mediated α -Fe₂O₃ particles on mesoporous carbon nanofibers as electrode materials with superior capacitive performance. *RSC Adv.* **2017**, *7*, 6818–6826. [[CrossRef](#)]
21. Nekoueian, K.; Amiri, M.; Sillanpaa, M.; Marken, F.; Boukherroub, R.; Szunerits, S. Carbon-based quantum particles: An electroanalytical and biomedical perspective. *Chem. Soc. Rev.* **2019**, *48*, 4281–4316. [[CrossRef](#)] [[PubMed](#)]
22. Wang, Z.B.; Zhang, C.L.; Xu, C.Q.; Zhu, Z.H.; Chen, C.N. Hollow polypyrrole nanosphere embedded in nitrogen-doped graphene layers to obtain a three-dimensional nanostructure as electrode material for electrochemical supercapacitor. *Ionics* **2017**, *23*, 147–156. [[CrossRef](#)]
23. Fedoseeva, Y.V.; Bulusheva, L.G.; Koroteev, V.O.; Mevellec, J.Y.; Senkovskiy, B.V.; Flahaut, E.; Okotrub, A.V. Preferred attachment of fluorine near oxygen-containing groups on the surface of double-walled carbon nanotubes. *Appl. Surf. Sci.* **2020**, *504*, 144357. [[CrossRef](#)]
24. Ge, T.; Min, F.F.; Zhang, M.X. A research into the nonthermal effect of thiophenic sulfur structure in the coking coal under microwave radiation. *Spectrosc. Spect. Anal.* **2018**, *38*, 3495–3501.
25. Cui, X.Q.; Cao, D.; Djellabi, R.; Qiao, M.; Wang, Y.; Zhao, S.; Mao, R.; Gong, Y.; Zhao, X.; Yang, B. Enhancement of Ni/NiO/graphitized carbon and beta-Cyclodextrin/reduced graphene oxide for the electrochemical detection of norfloxacin in water sample. *J. Electroanal. Chem.* **2020**, *851*, 113407. [[CrossRef](#)]
26. Ravulapalli, S.; Kunta, R. Enhanced removal of chromium (VI) from wastewater using active carbon derived from Lantana camara plant as adsorbent. *Water Sci. Technol.* **2018**, *78*, 1377–1389. [[CrossRef](#)]
27. Park, E.J.; Kim, H.J.; Han, S.W.; Jeong, J.H.; Kim, I.H.; Seo, H.O.; Kim, Y.D. Assembly of PDMS/SiO₂-PTFE and activated carbon fibre as a liquid water-resistant gas sorbent structure. *Chem. Eng. J.* **2017**, *325*, 433–441. [[CrossRef](#)]
28. Rao, K.T.V.; Souzanchi, S.; Yuan, Z.S.; Ray, M.B.; Xu, C.B. Simple and green route for preparation of tin phosphate catalysts by solid-state grinding for dehydration of glucose to 5-hydroxymethylfurfural (HMF). *RSC Adv.* **2017**, *7*, 48501–48511. [[CrossRef](#)]
29. Gromov, N.V.; Medvedeva, T.B.; Taran, O.P.; Bukhtiyarov, A.V.; Aymonier, C.; Prosvirin, I.P.; Parmon, V.N. Hydrothermal solubilization-hydrolysis-dehydration of cellulose to glucose and 5-hydroxymethylfurfural over solid acid carbon catalysts. *Top. Catal.* **2018**, *61*, 1912–1927. [[CrossRef](#)]
30. Shen, J.Y.; Zhang, L.; Ren, J.; Wang, J.C.; Yao, H.C.; Li, Z.J. Highly enhanced acetone sensing performance of porous C-doped WO₃ hollow spheres by carbon spheres as templates. *Sens. Actuators B* **2017**, *239*, 597–607. [[CrossRef](#)]
31. Jin, C.Q.; Zhu, K.X.; Peterson, G.; Jian, Z.Y.; Xu, G.; Wei, Y.X.; Ge, C.H.; Li, J.H. Morphology dependent photocatalytic properties of ZnO nanostructures prepared by a carbon-sphere template method. *J. Nanosc. Nanotechnol.* **2018**, *18*, 5234–5241. [[CrossRef](#)] [[PubMed](#)]
32. Wang, Y.; Jin, Y.H.; Zhao, C.C.; Pan, E.Z.; Jia, M.Q. 1D ultrafine SnO₂ nanorods anchored on 3D graphene aerogels with hierarchical porous structures for high-performance lithium/sodium storage. *J. Colloid. Interf. Sci.* **2018**, *532*, 352–362. [[CrossRef](#)] [[PubMed](#)]
33. Wang, F.; Liu, Y.; Zhao, Y.F.; Wang, Y.; Wang, Z.J.; Zhang, W.H.; Ren, F.Z. Facile synthesis of two-dimensional porous MgCo₂O₄ nanosheets as anode for lithium-ion batteries. *Appl. Sci. Basel* **2018**, *8*, 22.
34. Tao, T.; Lu, S.G.; Fan, Y.; Lei, W.W.; Huang, S.M.; Chen, Y. Anode improvement in rechargeable lithium-sulfur batteries. *Adv. Mater.* **2017**, *29*, 1700542. [[CrossRef](#)] [[PubMed](#)]
35. Lee, D.Y.; Ahn, S.H. Investigation of laser cutting width of LiCoO₂ coated aluminum for lithium-ion batteries. *Appl. Sci. Basel* **2017**, *7*, 914. [[CrossRef](#)]
36. Wang, Y.P.; Fu, Q.; Li, C.; Li, H.H.; Tang, H. Nitrogen and phosphorus dual-doped graphene aerogel confined monodisperse iron phosphide nanodots as an ultrafast and long-term cycling anode material for sodium-ion batteries. *ACS Sustain. Chem. Eng.* **2018**, *6*, 15083–15091. [[CrossRef](#)]

37. Li, F.; Song, H.M.; Yu, W.S.; Ma, Q.L.; Dong, X.T.; Wang, J.X.; Liu, G.X. Electrospun TiO₂//SnO₂ Janus nanofibers and its application in ethanol sensing. *Mater. Lett.* **2020**, *262*, 127070. [[CrossRef](#)]
38. Hermawan, A.; Asakura, Y.; Inada, M.; Yin, S. One-step synthesis of micro-/mesoporous SnO₂ spheres by solvothermal method for toluene gas sensor. *Ceram. Int.* **2019**, *45*, 15435–15444. [[CrossRef](#)]



© 2020 by the authors. Licensee MDPI, Basel, Switzerland. This article is an open access article distributed under the terms and conditions of the Creative Commons Attribution (CC BY) license (<http://creativecommons.org/licenses/by/4.0/>).